Received: 4 February 2023 | Revised: 19 March 2023 | Accepted: 20 March 2023

DOI: 10.1002/apj.2907

RESEARCH ARTICLE

Asia-Pacific Journal of Chemical Engineering | Curtin University | WILEY

Natural manganese ores for efficient removal of organic pollutants via catalytic peroxymonosulfate-based advanced oxidation processes

Zhengxin Yao[1] | Roufei Chen[1,2] | Ning Han[1,3] | Hongqi Sun[1,4] | Ngie Hing Wong[5] | Lusi Ernawati[6] | Shaobin Wang[1,7] | Jaka Sunarso[5] | Shaomin Liu[1]

[1]Western Australia School of Mines: Minerals, Energy and Chemical Engineering, Curtin University, Perth, Western Australia 6102, Australia

[2]School of Electro-mechanical Engineering, Zhongkai University of Agriculture and Engineering, Guangzhou 510225, China

[3]Department of Materials Engineering, KU Leuven, Leuven 3001, Belgium

[4]School of Science, Edith Cowan University, Joondalup, Western Australia 6027, Australia

[5]Research Centre for Sustainable Technologies, Faculty of Engineering, Computing and Science, Swinburne University of Technology, Jalan Simpang Tiga, 93350 Kuching, Sarawak, Malaysia

[6]Department of Chemical Engineering, Institut Teknologi Kalimantan, Balikpapan 76127, Indonesia

[7]School of Chemical Engineering and Advanced Materials, The University of Adelaide, Adelaide, South Australia 5005, Australia

Correspondence
Jaka Sunarso, Research Centre for Sustainable Technologies, Faculty of Engineering, Computing and Science, Swinburne University of Technology, Jalan Simpang Tiga, 93350 Kuching, Sarawak, Malaysia.
Email: barryjakasunarso@yahoo.com; jsunarso@swinburne.edu.my

Funding information
Australian Research Council, Grant/Award Number: DP180103861

Abstract

Peroxymonosulfate-based advanced oxidation processes (PMS-AOPs) for in situ persistent organic pollutant (POP) remediation in aqueous solutions can be a promising technology. However, this technology is constrained by its high toxicity and cost of metal oxide and non-metal catalysts for PMS activation. Here, we investigated the catalytic performance of a widely available natural mineral, manganese ore (MO), for PMS activation. A series of natural MO samples in an aqueous solution were prepared via the Fenton-like reaction. The samples' crystalline structure, surface morphology, textural properties, and other surface characteristics of the selected MO were systematically characterized. The effects of PMS concentration and process parameters on the degradation performance of four chosen model pollutants, that is, phenol, tetrabromobisphenol A (TBBPA), rhodamine B (RhB), and methylene blue (MB), were evaluated. The experimental results showed that natural MO increased catalytic activity and enhanced the PMS oxidation processes, with 98%, 90%, and 75% removal efficiencies on phenol, TBBPA, and RhB, respectively, within 1.5 h. The reduction in the initial pH solution from 10 to 7 and the increase in temperature from 15 to 45°C enhanced the MB degradation rate (decolorization) by 55 and 46%, respectively, within 2 h. During the PMS activation process, $SO_4^{\bullet -}$, $^{\bullet}OH$, and $^1O_2$ species were generated, but only $SO_4^{\bullet -}$ and $^{\bullet}OH$ radicals

with strong oxidative potentials contributed to the catalytic degradation. The dissolved metals from the experiments were found well within the limit of drinking water standards, verifying that the MO + PMS catalytic system is suitable for commercial applications. This work provides insights into the development potential and prospects of using natural minerals for PMS activation and POP degradation, which can accelerate their industrial applications.

KEYWORDS

advanced oxidation processes, catalysts, peroxymonosulfate activation, persistent organic pollutants, sulfate radicals, water remediation

1 | INTRODUCTION

Rapid industrialization and continuous population growth have become global issues, leading to extensive environmental pollution, especially water pollution.[1,2] Persistent organic pollutants (POPs), contaminants notoriously known for their long-lasting and toxic existence in the environment, require urgent treatment solutions.[3–5] A peroxymonosulfate-based advanced oxidation process (PMS-AOP) is a promising in situ POP remediation technology in aqueous solutions, given its high efficiency and broad applicability.[6–8] As a commonly used oxidant, PMS shows excellent potential for POP degradation, given its low cost, nontoxicity, and chemical stability. However, PMS activation generally requires the presence of metal oxides as catalysts to generate sulfate radicals ($SO_4^{\cdot-}$) at high standard redox potential (2.5–3.1 V) for effective POP degradation.[9,10]

Applying metal catalysts that do not naturally exist requires complex synthetic pre-processing, which thus increases the cost of industrial applications.[11,12] Abundantly available natural mineral catalysts are worth exploring.[13–15] Natural transition metals and their compounds, such as iron (Fe), cobalt (Co), and manganese (Mn) ores, have demonstrated their excellent potential for PMS activation and POP degradation.[15,16] Natural ores are attractive for their low cost, abundant availability, and comparable performance to synthetic catalysts,[17] especially for Earth's 12th most abundant element, Mn.[18,19] Several Mn oxides, that is, Mn monoxide, Mn dioxide, and Mn trioxide, have displayed high catalytic performance in PMS-AOP systems and for POP degradation.[20,21] Similarly, natural Mn ore (MO) comprises various Mn compounds that may display good catalytic performance for POP degradation.

Four operating mines and one tailing retreatment plant in Australia produce millions of tonnages of MO and generate more than one billion Australian dollars' worth annually. Two of these four Mn mines are located in Western Australia, bringing this work unique geographical and cost advantages for large-scale application. This work aims to evaluate the catalytic performances of the widely available natural MOs for PMS activation. The crystalline structure, surface morphology, textural properties, and other surface characteristics of the selected MOs were characterized by powder X-ray diffraction (XRD), scanning electron microscope coupled with energy-dispersive spectrometry (SEM-EDS), Brunauer–Emmett–Teller (BET) specific surface area, Barrett–Joyner–Halenda (BJH) pore size distribution, and X-ray photoelectron spectroscopy (XPS). The effects of PMS concentration and other process parameters on the degradation performances of four model pollutants, that is, phenol, tetrabromobisphenol A (TBBPA), rhodamine B (RhB), and methylene blue (MB), were evaluated, including their removal efficiencies in relation to the initial pH value of the solutions and reaction temperatures. Furthermore, electron paramagnetic resonance (EPR) and selective radical quenching experiments were conducted to reveal the catalytic mechanisms in the PMS-AOP system.

2 | MATERIALS AND METHODS

2.1 | Chemicals and materials

Table 1 shows the composition of the selected MO samples supplied by Karara Mining Ltd. and OM Manganese Pty. Ltd., Australia. Two batches of commercially tested MO powder samples were obtained from the same mine, and each batch contained four samples. The first four samples from first batch and the next four samples from second batch were labeled as MO-1 to MO-8 consecutively. Before the experiments, the MO samples were ultrasonically cleaned with deionized (DI) water. Then, we manually sieved the samples to remove non-stone components such as organic matter and filtered them

TABLE 1 The composition of manganese ore (MO) samples supplied by the mining companies.

Composition	Formula	Content (wt.%)
Braunite	$4MnO_3{\cdot}3MnO_2{\cdot}SiO_2$	30%
Psilomelane	$Ba{\cdot}Mn{\cdot}Mn_8O_{16}(OH)$	30%
Pyrolusite	MnO_2	30%
Quartz	SiO_2	10%

with filter paper. Afterward, we dried the samples in an oven at 105°C for 12 h and then further sieved them to obtain 50–60 μm particles for subsequent tests.

Next, we purchased four chosen model pollutants, that is, phenol (≥99%), TBBPA (≥99%), RhB (≥99%), and MB (≥99%), and two spin-trapping agents, that us, 5,5-dimethyl-1-pyrroline (DMPO, ≥99%), and 2,2,6,6-tetramethyl-4-piperidinol (TMP, ≥99%), from Sigma-Aldrich. A series of diluted model pollutants using DI water was prepared for pollutant degradation experiments. Given the low solubility of TBBPA under pH 7, we added NaOH (0.1 M) to the solution to adjust the pH value to 11 for producing the TBBPA solution.

2.2 | Preliminary MO degradation experiments

We systematically conducted the preliminary degradation experiments using the prepared MO-1 to MO-8 catalysts with and without PMS activation. These preliminary experiments included eight control (MO only) groups and eight variable (MO + PMS) groups. They were conducted once only to screen the initial samples, compare their catalytic performances, and find the representative MO type for the MO + PMS system. Then, we repeated the subsequent experiments more than three times to obtain reliable results. Firstly, a 500-mL beaker as a reactor carrying 200-mL model pollutant (i.e., 20 ppm phenol) was placed in a thermostatic water bath with a mechanical stirrer to maintain homogenous solution conditions throughout the reaction. Then, we added 1 g L^{-1} MO and 2 g L^{-1} PMS to the beaker with the pollutant solution under controlled conditions (pH 7 and 25°C) to initiate the oxidation reaction. However, the MO catalyst was added before PMS for adsorption, and the reaction timing was recorded from the time of PMS addition.

During the experiment, we collected 1 mL of solution periodically, filtered with the 0.45 μm polytetrafluoroethylene (PTFE) membrane, and mixed immediately with 0.5 mL of methanol to quench the oxidation. An ultra-high-performance liquid chromatography (UHPLC, Thermo Fisher Scientific UltiMate 3000) with a UV–visible spectrophotometer (JASCO) set at 270 nm was used to measure the residual phenol concentration.[22] We repeated these experiments three times to ensure the reliability and validity of the degradation experiment. Then, we evaluated their kinetic reaction rates of the phenol degradation using Equation (1), where k (min^{-1}) represents the first-order kinetic reaction rate constant of the contaminant degradation,[23] C_t and C_o are the concentration at the reaction time, t, and the initial concentration of chosen pollutants, respectively.

$$\ln(C_t/C_o) = -kt \quad (1)$$

2.3 | Characterization of chosen MO catalyst

To investigate the morphology and microstructure of the chosen MO catalyst, we employed the following equipment and procedures: (a) scanning electron microscopy (SEM, FESEM Zeiss Neon 40EsB) coupled with an energy-dispersive X-ray spectroscopy (EDS) for probing the sample's surface morphology; the sample was tested with carbon glue on the holder to ensure electrical conductivity; the applied SEM and EDS voltages were about 15 and 20 kV, respectively; EDS scanning was conducted to exclude carbon elements in the complete element scanning to avoid carbon-containing tape interference; we also repeated this test several times to obtain reliable results; (b) powder X-ray diffraction (XRD, Bruker D8 Advance) using Cu-Kα radiation at 40 kV and 30 mA with the step size and time of 0.02° (2θ) and 0.01 s, respectively, to determine the sample's crystalline structure; then, the recorded powder XRD patterns were identified and intepreted by referring to the standard spectra (JCPDS-ICDD) in its software; this test was repeated twice for obtaining reliable results; (c) X-ray photoelectron spectroscopy (XPS, Thermo Escalab 250) using Al-Kα X-ray radiation for determining surface chemical composition; the deconvolution of obtained XPS spectra was carried out using Voigt functions with a 30% Lorentzian component after baseline subtraction using the Shirley method; and (d) surface area analyzer (Micromeritics TriStar II Plus) for measuring the textural properties by N_2 adsorption at −196°C, the sample of which needs be degassed first by evacuation at 250°C for 12 h; the test was repeated four times for obtaining reliable average values by using a new powder sample each time. We also measured the sample's specific surface area (SSA) using the Brunauer–Emmett–Teller (BET) model and pore size distribution (PSD) using the Barrett–Joyner–Halenda (BJH) model.

2.4 | Catalytic activity experiments

Based on the aforementioned preliminary results, we performed similar degradation experiments for TBBPA, RhB, and MB using the chosen MO catalyst to evaluate the effects of PMS activation under different conditions. These conditions included adding (a) 0.3 g L^{-1} PMS only, (b) 0.5 g L^{-1} chosen MO catalyst only, and (c) a combination of MO + PMS under 25°C and pH 11 or 7 for 20 ppm of TBBPA or RhB model pollutants, respectively. Moreover, we repeated the degradation experiments for TBBPA using different PMS dosages ranging from 0.1 to 0.3 g L^{-1} under 25°C and pH 11 and constant MO (0.5 g L^{-1}). Then, we also evaluated their corresponding degradation kinetic reaction rates using Equation (1) to determine the optimal PMS dosage for the subsequent experiments. On the other hand, we performed the same degradation experiment using MB as the model pollutant based on the chosen MO and optimal PMS dosage but under different initial pH values (i.e., 7, 9, and 10) and different reaction temperatures (i.e., 15, 25, 35, and 45°C). For measuring TBBPA, RhB, and MB residual concentrations, we set the UV–visible spectrophotometer at 464, 554, and 664 nm, respectively.[22,24,25] Similarly, we evaluated their corresponding degradation kinetic reaction rates using Equation (1) to determine the optimal pH and reaction temperature conditions.

2.5 | Radical quenching experiments

We conducted selective radical quenching experiments to demonstrate the MO catalytic mechanisms in the PMS-AOP system. Firstly, we filtered the collected sample solution (1 mL) using the 0.45 μm PTFE membrane and mixed it with an indicator immediately for electron paramagnetic resonance (EPR) analysis every 5 min to detect the free radicals during the experiments. A Bruker EMX-E spectrometer was utilized using DMPO and TMP as spin-trapping agents under 3510 G centerfield, 100 G sweep width, and 100 GHz modulation frequency testing conditions. These experiments were conducted similarly to the degradation experiments but under different conditions. The reaction conditions used for the in situ EPR tests consisted of (a) catalyst loading (0.5 g L^{-1}), (b) PMS loading (0.3 g L^{-1}), (c) pH 7.0, (d) 8 mM of DMPO, and (e) 0.08 mM of TMP.[26] At the end of the experiment, we collected another 10 mL of the sample solution. We filtered it with the same PTFE membrane filter before testing it using inductively coupled plasma mass spectrometry (ICP-MS, PerkinElmer, Elan DRC-e) to measure the trace metal elements. Lastly, we also prepared standard solutions to obtain standard concentration curves.

3 | RESULTS AND DISCUSSION

3.1 | Representative MO + PMS system

Figure 1 shows phenol degradation using eight MO samples (MO-1 to MO-8) with and without PMS oxidation to determine the representative MO + PMS system for the subsequent experiments. Firstly, we noticed that all the samples exhibited phenol degradation but with different variations. All the samples without PMS (MO-1 to MO-8 only) rapidly reached an adsorption–desorption process in the first 15 min, with only about 10% of phenol removal in the absence of PMS. This result can be ascribed to the limited SSA (12.6 m^2 g^{-1}) of the MO

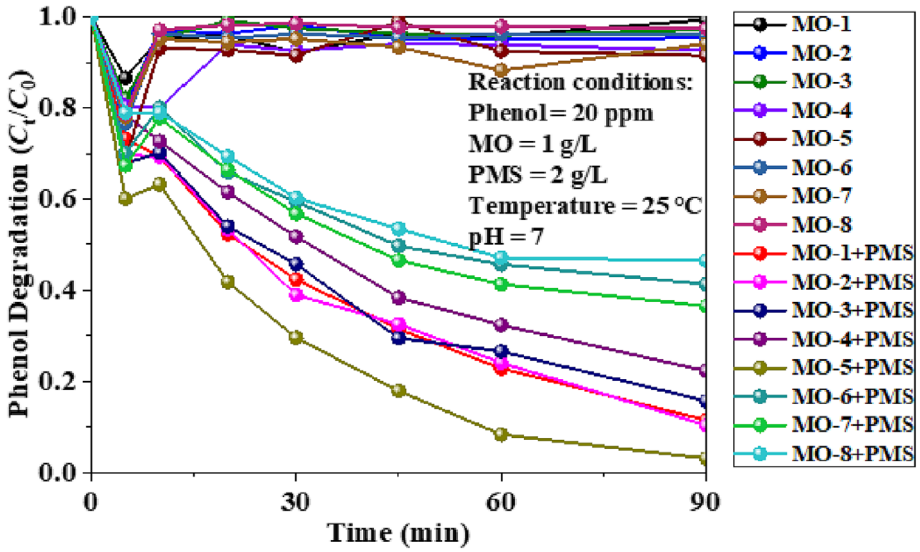

FIGURE 1 Effect of MO catalysts on phenol degradation with and without PMS activation.

catalysts. After adding PMS to the experiments, different MO + PMS systems achieved 52%–98% phenol degradation within 90 min (Table 2). Among them, MO-5 + PMS exhibited the highest phenol degradation (98%), and the other seven systems presented in the descending order of MO-2 + PMS < MO-1 + PMS < MO-3 + PMS < MO-4 + PMS < MO-7 + PMS < MO-6 + PMS < MO-8 + PMS. These variations can also be ascribed to different batches of samples collected from the same mine and their differences in microstructure properties and chemical composition, which we verified in the subsequent experiments. On the other hand, several other studies reported that their advanced oxidation process (AOP) systems revealed little phenol degradation when only using PMS (without catalysts).[27–30] We thus deduced that both MO and PMS (MO + PMS) were necessary for achieving significant phenol degradation in an AOP system. As a result, we chose the MO-5 + PMS system as the representative AOP system for the subsequent experiments.

3.2 | Characterization of chosen MO-5 catalyst

Figure 2 displays the SEM with EDS mapping images to characterize the MO-5 catalyst's surface morphology and chemical composition. Several fine particles were observed on the MO sample, suggesting that they were

TABLE 2 The removal efficiencies of MO catalysts for PMS activation on phenol degradation within 90 min.

MO + PMS experiments	MO-1 + PMS	MO-2 + PMS	MO-3 + PMS	MO-4 + PMS	MO-5 + PMS	MO-6 + PMS	MO-7 + PMS	MO-8 + PMS
Removal efficiency (%)	89	90	82	78	98	58	62	52

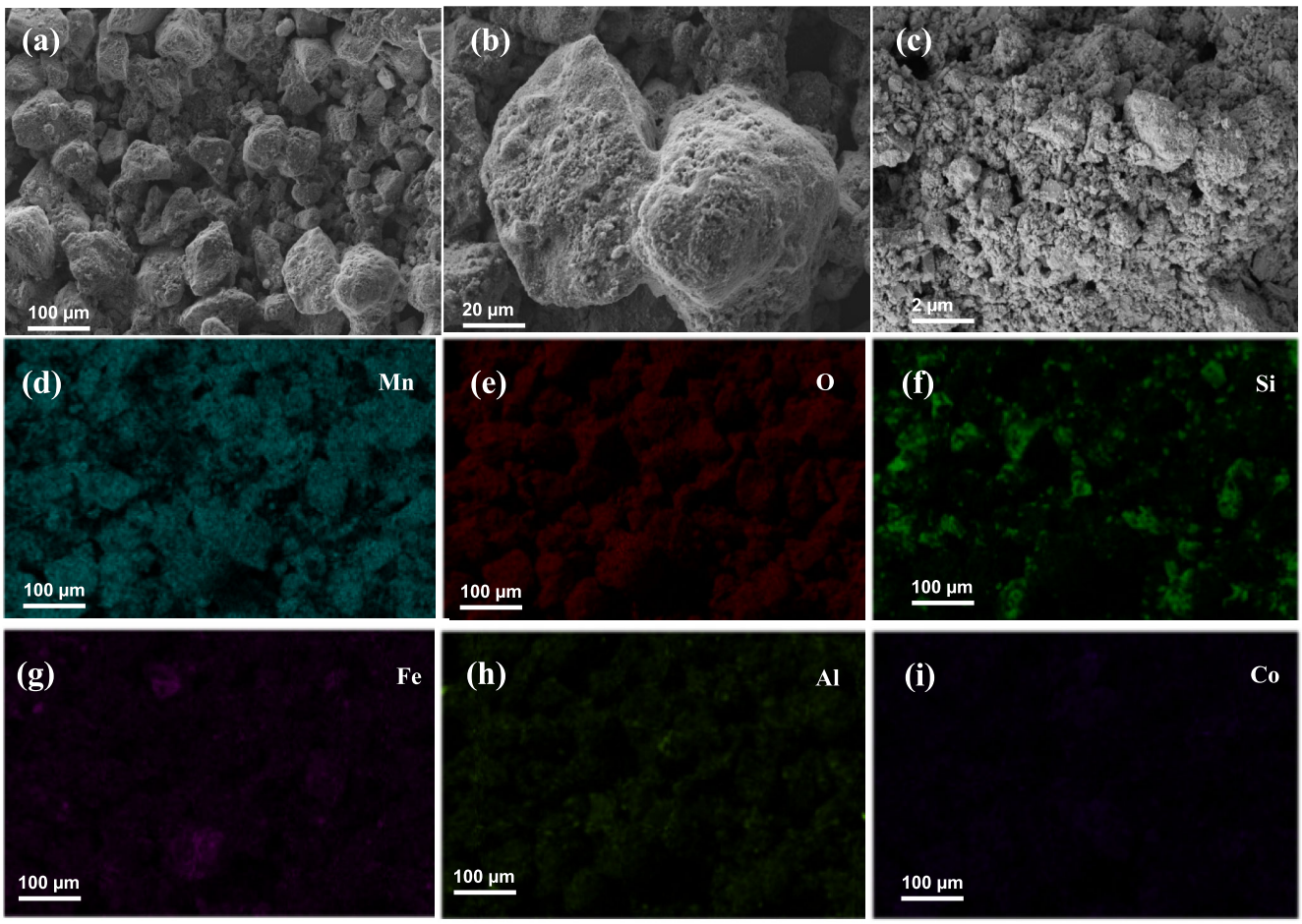

FIGURE 2 (a–c) SEM images of MO-5 catalyst at different magnifications. EDS mapping images of (d) MI (e) O, (f) Si, (g) Fe, (h) Al, and (i) Co on the catalyst sample.

responsible for the sample's magnetism property (Figure 2a–c). To further verify the sample's magnetic properties, we used a magnet to test the sample with a transparent container. We found that the magnet attracted part of the powder sample. This result can be ascribed to the different compositions in the sample, such as iron (Fe), which typically has magnetic properties. Due to the complex composition of the MO, it may contain a similar composition of magnetite (Fe ore).[28] Such magnetic properties could benefit catalyst recovery.

Besides, the EDS mapping images show that Mn appeared to be the most abundant element in the sample (Figure 2d–i). We also noticed a certain amount of O (Figure 2e) and Si (Figure 2f) from metallic oxides and silicon dioxide sources in the sample, matching the compositions derived from the natural ore. Since SiO_2 can be commonly found in sand and stone, finding Si and O in natural ore samples is reasonable. A small amount of Fe was also detected in the MO sample (Figure 2g). This result can be ascribed to the Fe ore being the largest ore resource in Australia and thus often being detected in other ores.[31] Lastly, a minor quantity of Co was detected (Figure 2i), which may play a significant role in the catalytic system.[32,33] Shukla et al[34] reported that Co_3O_4–SiO_2, potential main constituents of MO, could completely degrade phenol in 190 min. In short, the main active ingredients for the MO sample were identified as MnO_2, Fe_2O_3, CoO, and Co_3O_4.

Figure 3a displays the powder XRD patterns of the MO-5 sample for characterizing its crystalline structures. We noticed characteristic peaks at 2θ of 21°, 27°, 37°, 39°, 51°, 60°, 58°, 76°, and 82° that can be indexed to quartz crystal planes.[35] Moreover, the diffraction peaks at 2θ of 24°, 33°, 36°, 41°, and 55° matched the pyrolusite crystal planes of MnO_2.[36] Lastly, the diffraction peaks at 2θ of 28°, 38°, 43°, 47°, and 57° also matched those of the hematite Fe_2O_3.[37] Table 1 reveals that the total Mn content in the natural MO samples was nearly 30% and consisted of various Mn-containing compounds. Such characteristics with different Mn species in the natural MO may result in diverse catalytic efficiency. Hence, we investigated phenol degradation by adding PMS without a catalyst and found no oxidation reaction. In contrast, we discovered phenol degradation when adding different Mn oxide catalysts and oxidants (PMS) simultaneously. As a result, Mn_2O_3 exhibited the most effective PMS activation and yielded sulfate radicals ($SO_4^{\cdot-}$). Hence,

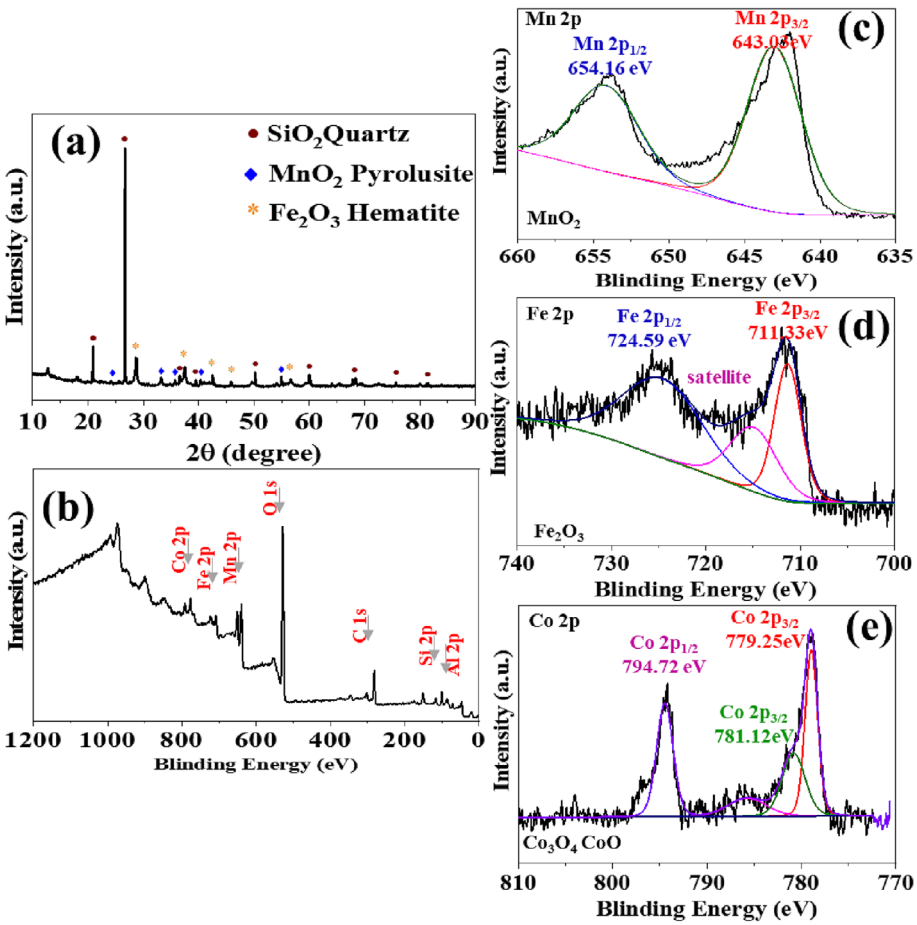

FIGURE 3 (a) Powder XRD patterns of MO-5 sample; (b) a full XPS survey spectra; and deconvoluted spectra of (c) Mn 2p, (d) Fe 2p, and (e) Co 2p of MO-5 sample.

compared to MnO–PMS (90%), Mn_3O_4–PMS (66.4%), and MnO_2–PMS (61.5%) of phenol removal in 2 h, Mn_2O_3–PMS exhibited 100% phenol degradation in 1 h. These results also verified the Mn oxide catalysts performed in the following order: Mn_2O_3 > MnO > Mn_3O4 > MnO_2,[28] and divalent manganese (Mn^{2+}) was dominant in the natural MO, as indicated in Table 1.

The XPS survey spectra indicated that various metal elements, including Co, Fe, Mn, and Al, were present on the MO surface (Figure 3b). The two peaks from the Mn 2p spectrum located at 643.03 and 654.16 eV demonstrate the existence of MnO_2 (Figure 3c).[38–40] Similarly, the two peaks at 711.33 and 724.59 eV from the Fe 2p spectrum indicated the presence of Fe_2O_3 (Figure 3d).[41–43] Lastly, the three peaks at 779.25, 781.12, and 794.72 eV from the Co 2p spectrum indicated that Co existed as both Co_3O_4 and CoO on the MO surface (Figure 3e).[44–46] Due to the presence of different chemicals in the samples, the peaks were superimposed on the XPS images. Although we corrected them in the imaging program, they still differed slightly from the standard references. Besides that, based on the BET and BJH analyses, the SSA and average pore size for the MO-5 sample were 12.6 m^2 g^{-1} and 7.4 mm, respectively. This result showed a lower SSA than synthetic porous catalysts or nanomaterials, typically in hundreds of SSA.[14,34,39] However, as natural minerals, this lower SSA of MO-5 is acceptable since it exhibited efficient reactions.

3.3 | Effects of PMS on TBBPA and RhB degradation

Figure 4 shows TBBPA and RhB degradation based on constant and different PMS concentrations in the presence and absence of MO (5 g L^{-1}). PMS or MO only exhibited low TBBPA degradation (10%–20%) under alkaline conditions (pH 11) (Figure 4a). In contrast, the TBBPA degradation increased and reached nearly 99% within 1 h in MO + PMS. Similarly, the RhB degradation increased from nearly 2%–75% within 1 h in MO + PMS against MO or PMS only under neutral pH (Figure 4b). In other words, using MO or PMS alone cannot produce significant degradation effects.[28–30]

The influence of PMS dosages, that is, 0.1, 0.2, and 0.3 g L^{-1}, on TBBPA degradation was investigated with

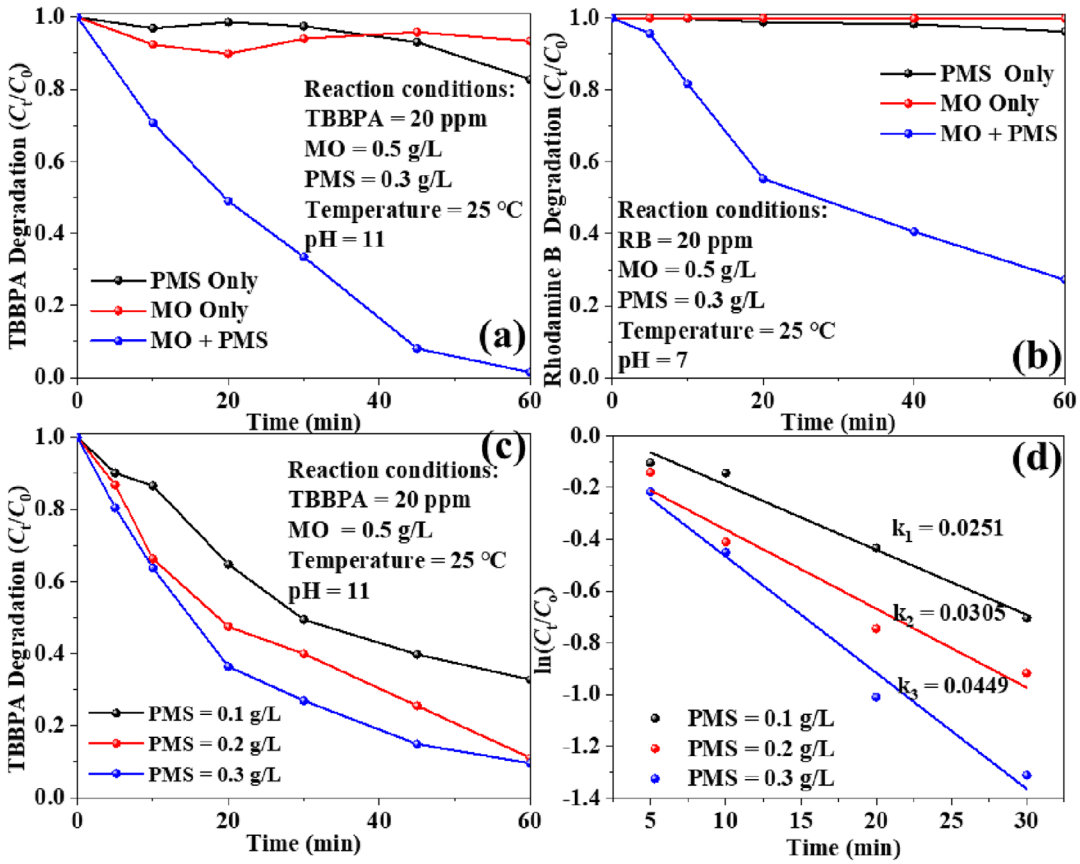

FIGURE 4 Effect of PMS with and without MO catalyst on (a) TBBPA degradation and (b) RhB degradation. (c) Effect of different PMS concentrations on TBBPA degradation under the specified reaction conditions and (d) their matching first-order kinetic reaction rates.

0.5 g L^{-1} of MO under alkaline conditions (Figure 4c). A positive correlation of TBBPA removal efficiency with PMS concentration was obtained, that is, 60% (0.1 g L^{-1}), 88% (0.2 g L^{-1}), and 90% (0.3 g L^{-1}) within 1 h. Although the 0.2 and 0.3 g L^{-1} PMS systems reached similar removal efficiency at 1 h, their first-order kinetic reaction rate constants (k, min^{-1}), as calculated using Equation (1), exhibited a significant difference, that is, 0.2 g L^{-1} ($k_2 = 0.0305\ min^{-1}$) and 0.3 g L^{-1} ($k_3 = 0.0449\ min^{-1}$) (Figure 4d). In short, the 0.3 g L^{-1} ($k_3 = 0.0449\ min^{-1}$) PMS system showed a higher reaction rate than the 0.2 g L^{-1} ($k_2 = 0.0305\ min^{-1}$) and 0.1 g L^{-1} ($k_1 = 0.0251\ min^{-1}$) PMS systems.

3.4 | Effects of initial pH solution on MB degradation

Figure 5 shows the effect of the initial pH solution, that is, 7, 9, and 10, on MB degradation with 0.1 g L^{-1} for both MO and PMS. Since site pollution is typically accompanied by land salinity, the pollutant degradation performance in an alkaline environment is critical for in situ remediation application. McAvoy et al[47] reported that the TBBPA solubility in water increased with pH, for example, 0.148 mg L^{-1} (pH 5), 1.26 mg L^{-1} (pH 7), and 2.34 mg L^{-1} (pH 9). The MB degradation rate increased with increased initial pH values, that is, 40% (pH 7), 50% (pH 9), and 95% (pH 10) (Figure 5a). Thus, the kinetic reaction rates increased with increased pH, that is, pH 7 ($k_1 = 0.0056\ min^{-1}$), pH 9 ($k_2 = 0.0112\ min^{-1}$), and pH 10 ($k_3 = 0.0311\ min^{-1}$). These results suggested that more hydrogen ions (lower pH) could consume sulfate ($SO_4^{\cdot-}$) and hydroxyl ($^{\cdot}OH$) radicals, reducing the pollutant degradation capacity.[48,49]

3.5 | Effects of reaction temperature on MB degradation

Figure 6 shows the influence of different reaction temperatures, that is, 15, 25, 35, and 45°C, on MB degradation with 0.1 g L^{-1} for both MO and PMS. We tested the degradation with these temperatures since they represented the variation in different sewage treatments or other commercial applications. The MB degradation rate (decolorization) increased with reaction temperatures, that is, 37% (15°C), 42% (25°C), 62% (35°C), and 83% (45°C) (Figure 6a). Moreover, the reaction rates increased with increased temperature, that is, 15°C ($k_1 = 0.0045\ min^{-1}$), 25°C ($k_2 = 0.0056\ min^{-1}$), 35°C ($k_3 = 0.0099\ min^{-1}$), and 45°C ($k_4 = 0.0231\ min^{-1}$). In other words, a higher temperature could give rise to an increase in energy absorption for the O–O breaksup, thus activating the PMS.

3.6 | Catalytic mechanisms

Based on the previous studies,[50–56] the PMS activation by MO catalyst likely follows Equations (2)–(10):

$$HSO_5^- + \equiv Fe^{3+} \rightarrow \equiv Fe^{2+} + SO_5^{\cdot-} + H^+ \quad (2)$$

$$HSO_5^- + \equiv Fe^{2+} \rightarrow SO_4^{\cdot-} + OH^- + \equiv Fe^{3+} \quad (3)$$

$$HSO_5^- + \equiv Mn^{3+} \rightarrow \equiv Mn^{2+} + SO_5^{\cdot-} + H^+ \quad (4)$$

$$HSO_5^- + \equiv Mn^{2+} \rightarrow SO_4^{\cdot-} + OH^- + \equiv Mn^{3+} \quad (5)$$

$$SO_4^- + \equiv Co^{2+} \rightarrow \equiv Co^{3+} + SO_4^{2-} \quad (6)$$

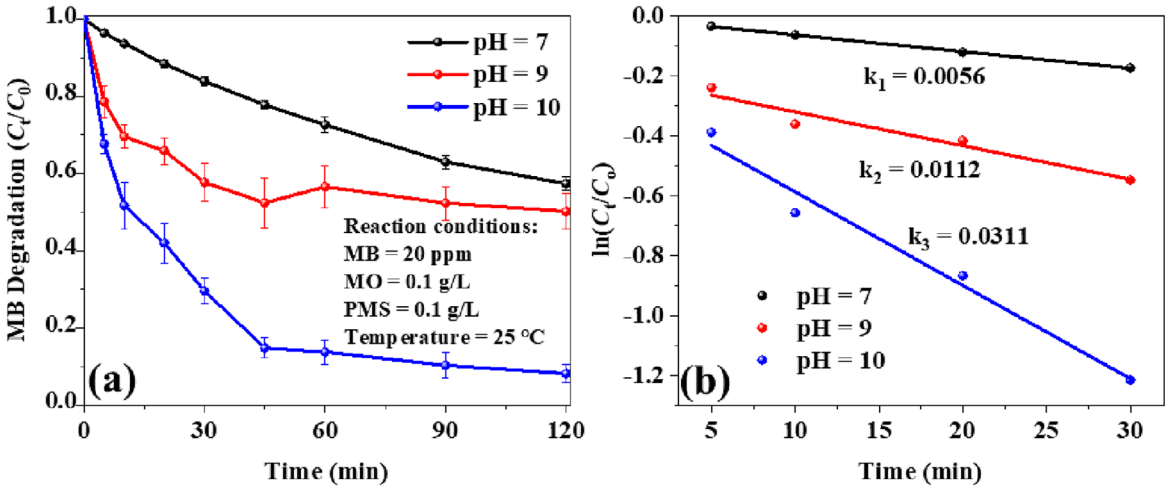

FIGURE 5 (a) Effect of initial solution pH on MB degradation and (b) their corresponding first-order kinetic reaction rates.

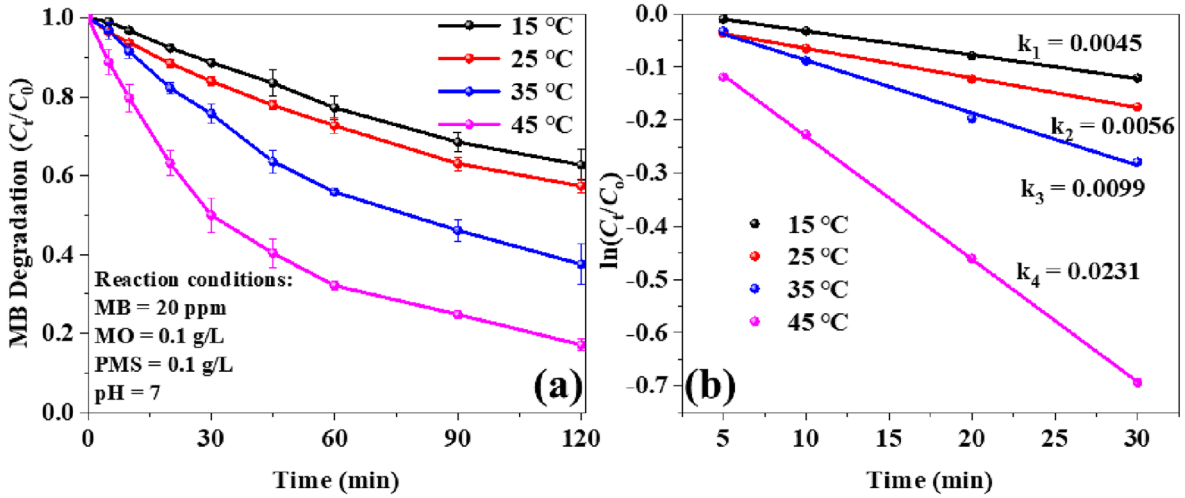

FIGURE 6 (a) Effect of different temperatures on MB degradation and (b) their matching first-order kinetic reaction rates.

FIGURE 7 EPR spectra of PMS activation with MO for detecting the presence of DMPO-sulfate ($SO_4^{\cdot -}$) and DMPO-hydroxyl ($^{\cdot}OH$) radicals.

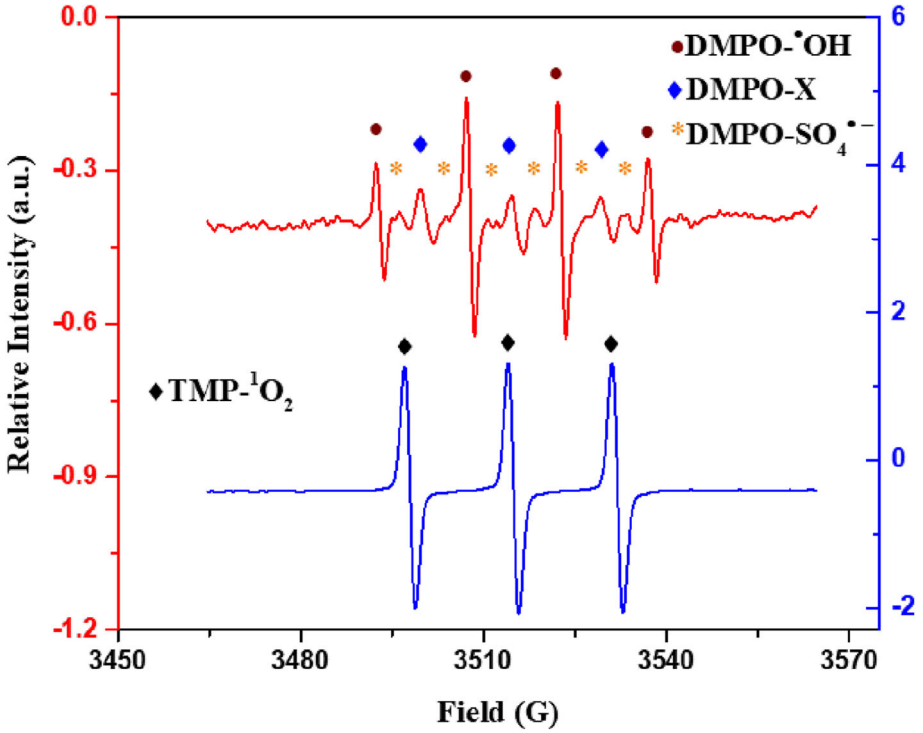

$$HSO_5^- + \equiv Co^{2+} \rightarrow SO_4^{\cdot -} + OH^- + \equiv Co^{3+} \quad (7)$$

$$SO_5^{\cdot -} + SO_5^{\cdot -} \rightarrow 2SO_4^{\cdot -} + {}^1O_2 \quad (8)$$

$$SO_4^{\cdot -} + H_2O \rightarrow H^+ + {}^{\cdot}OH + SO_4^{2-} \quad (9)$$

$$\text{Organic pollutants} + (SO_4^{\cdot -}/{}^{\cdot}OH) \rightarrow \text{degraded products}\ (CO_2 + H_2O + SO_4^{2-}) \quad (10)$$

Figure 7 shows the EPR spectra to detect the presence of DMPO–sulfate ($SO_4^{\cdot -}$) and DMPO–hydroxyl ($^{\cdot}OH$) radicals in the mixture solution to gain insights into the PMS activation mechanisms. The reaction conditions used in the in situ EPR tests consist of (a) MO catalyst loading (0.5 g L^{-1}), (b) PMS loading (0.3 g L^{-1}), (c) pH 7.0, (d) 8 mM of DMPO, and (e) 0.08 mM of TMP. For DMPO-$SO_4^{\cdot -}$ and DMPO-$^{\cdot}OH$ signals. At the beginning of the reaction, we noticed a quartet with an intensity ratio of 1:2:2:1 in the MO + PMS system. For the TMP–$^1O_2$ signal, we observed a similar triplet in this bauxite ore/PMS composite system at the beginning of the reaction, indicating $SO_4^{\cdot -}$ and $^{\cdot}OH$ radicals and singlet oxygen ($^1O_2$) were generated during PMS activation.

These species could oxidize organic pollutants is a typical system reaction feature.[26] Besides, $SO_4^{\cdot-}$ was rapidly consumed during oxidation indicated its participation during the reaction.

On the other hand, our EPR results also matched the peaks observed in previous studies based on synthesized catalysts and accorded well with the aforementioned mechanisms in Equations (2)–(10).[50–56] However, based on our aforementioned SEM and powder XRD results, several transition-metal elements and metal oxides were identified in our natural mineral samples, suggesting that these metal oxides may also activate PMS to degrade POPs. In short, the catalytic degradation mechanism of our natural metal minerals was consistent with that of synthetic metal catalysts, thus suggesting natural metal materials can be a suitable replacement for synthetic catalysts. However, due to the complex composition of our natural mineral samples, the specific mechanism requires further investigation and clarification in future studies.

3.7 | Water quality evaluation

Table 3 shows the ICP-MS results of the four metal residues after being degraded by the MO + PMS system with 20 ppm phenol. We adopted the World Health Organization (WHO) and European Union (EU) drinking water standards to compare the results since no single standard contains all four metal elements. Besides, we used the lower limits in both standards when the limits existed in both standards. All four metals met the standard requirements, suggesting that metal leaching in the MO + PMS system is relatively low and that this technology can be environmentally compatible with its commercial applications.

Table 4 lists the prices of the main components of the transition-metal catalysts for conducting a financial feasibility study and demonstrating the comparative advantages of natural ore and synthetic transition-metal catalysts in large-scale soil in situ remediation. The prices of chemical products were derived from the price of metal elements provided by Sigma-Aldrich to represent the estimated cost of the primary raw materials required for the laboratory catalyst synthesis. The price of industrial metal smelting products refers to the average time-sharing price of the spot trading market in China. Notably, China is the largest producer of steel and metal finished products. Shipping ore is generally used as industrial raw materials. It represents the lowest raw material price of laboratory-grade synthetic catalysts. The price of shipping ore was taken from the estimated price of the international ore futures trading market.

Due to the classification of ore with different purity, we used the highest purity refined ore as the price index so that our ore price is higher than the actual situation. As a result, the price of chemicals is two orders of magnitude higher than that of industrial metal smelting products (Table 4). Even cobalt, a rare element, has a chemical price four times higher than that of metal. The price of common metals is five times that of bulk refined ore, and the price of the rare metal cobalt ore is only 3% of its metal price. In making synthetic metal catalysts, many additional chemical products are required. Therefore, the actual catalyst raw material price difference must be higher. This is because most industrial or laboratory chemicals used in this process are more expensive than ordinary metal products. For example, the raw material cost of the synthetic catalyst exceeded 2000 Australian dollars, while the finished product we synthesized was less than 500 g.[53] In addition, synthetic catalysts require a lot of chemical experiment equipment, including but not limited to a muffle furnace, high-pressure reactor, and fume hood. Considering the cost of various consumables and equipment in the process, the current price of transition-metal catalysts is about thousands of Australian dollars per kilogram. Even if industrialized production significantly reduces manufacturing costs, its price can still be hundreds of times that of natural metal ore catalysts. Therefore, natural metal ore catalysts have incomparable financial advantages in activating PMS to degrade organic pollutants in large-scale soil remediation.

TABLE 4 The prices of the main components of the transition-metal catalysts.

Price (AUD kg^{-1})	Fe	Mn	Co
Analytical reagents	71	238	1088
Industrial metal	0.60	2	267.5
Shipping ore	0.15	0.41	7.94

Element (ppm)	Fe	Mn	Ca	Mg
MO + PMS system with [Phenol] = 20 ppm	0.1	0.01	1.1	4.2
Drinking water standards[57,58]	0.3	0.05	61	25

TABLE 3 Comparison of ICP-MS results on the MO + PMS treated water residues with drinking water standards.

4 | CONCLUSION

This work proposes an in situ wastewater remediation strategy by directly utilizing natural MO as the catalyst in PMS activation to remove organic pollutants via advanced oxidation processes. The MO-5 + PMS catalytic system performed well during the oxidative degradation of different contaminants, including phenol, TBBPA, RhB, and MB. Notably, TBBPA could be removed by up to 90% using the MO + PMS at 25°C and pH 11 within 1 h. The degradation efficiency revealed a positive correlation with PMS concentration. In contrast, a further increase in PMS concentration could not significantly affect degradation efficiency after it reached a maximum level. Increasing the reaction temperature from 15 to 45°C enhanced the MB degradation rate. The reduction in the initial pH solution from 10 to 7 increased the MO + PMS catalytic performance. The MO-5 sample could remove more than 50% of contaminants within 1.5 h, even under less favorable conditions, that is, at pH 7 and low temperature.

Moreover, EPR spectra revealed that $SO_4^{\bullet-}$, $^{\bullet}OH$, and $^1O_2$ radicals were generated during the PMS activation process for the catalytic degradation of organic pollutants. The ICP-MS demonstrated that the metals precipitated in the experiment were far below the limit of drinking water standards. Unsmelted ores are inexpensive and can come from many sources, so this work demonstrates the feasibility and potential of using natural ores for large-scale environmental remediation. Besides, the source of natural ore catalysts is not limited to commercial ores. Tailings mines are also a potential source. However, due to equipment limitations, this work could not standardize the ore screening process for the degradation tests, which warrants more thorough research with more samples in the future. Hence, at this stage, simulation experiments can be used to screen available ores, which can be integrated into the process of commodity ore detection. At the same time, ores have the potential to be substituted in most existing metal/PMS degradation systems so that the potentially degradable pollutants in this system can be diverse.

ACKNOWLEDGEMENTS

The authors gratefully acknowledge funding support from the Australian Research Council Discovery Project (DP180103861). The authors are grateful to Karara Mining Ltd. and OM Manganese Pty. Ltd, Australia, which provided the ore samples. The authors also want to thank the technical assistance from Roshanak Doroushi, Veronica Avery, Xiao Hua, and Hillary Christensen Ho Zhen Hui. The authors also thank the John de Laeter Centre for SEM, XRD, and XPS at Curtin University. Open access publishing facilitated by Swinburne University of Technology, as part of the Wiley - Swinburne University of Technology agreement via the Council of Australian University Librarians.

CONFLICT OF INTEREST STATEMENT

The authors declare no known competing financial interests or personal relationships that could have appeared to influence the work reported in this paper.

ORCID

Zhengxin Yao https://orcid.org/0000-0002-3391-6475
Ngie Hing Wong https://orcid.org/0000-0003-0116-5272
Jaka Sunarso https://orcid.org/0000-0002-5234-7431

REFERENCES

1. Singh VP. Water, environment, engineering, religion, and society. *J Hydrol Eng*. 2008;13(3):118-123. doi:10.1061/(ASCE)1084-0699(2008)13:3(118)
2. Ebenstein A. The consequences of industrialization: evidence from water pollution and digestive cancers in China. *Rev Econ Stat*. 2012;94(1):186-201. doi:10.1162/REST_a_00150
3. Jones KC, De Voogt P. Persistent organic pollutants (POPs): state of the science. *Environ Pollut*. 1999;100(1-3):209-221. doi:10.1016/S0269-7491(99)00098-6
4. Wania F, Mackay D. Peer reviewed: tracking the distribution of persistent organic pollutants. *Environ Sci Technol*. 1996;30(9):390A-396A. doi:10.1021/es962399q
5. Vallack HW, Bakker DJ, Brandt I, et al. Controlling persistent organic pollutants–what next? *Environ Toxicol Phar*. 1998;6(3):143-175. doi:10.1016/S1382-6689(98)00036-2
6. Zhi D, Lin Y, Jiang L, et al. Remediation of persistent organic pollutants in aqueous systems by electrochemical activation of persulfates: a review. *J Environ Manage*. 2020;260:110125. doi:10.1016/j.jenvman.2020.110125
7. Zhao Q, An J, Wang X, Li N. In-situ hydrogen peroxide synthesis with environmental applications in bioelectrochemical systems: a state-of-the-art review. *Int J Hydrogen Energy*. 2021;46(4):3204-3219. doi:10.1016/j.ijhydene.2020.05.227
8. Yang Q, Ma Y, Chen F, et al. Recent advances in photo-activated sulfate radical-advanced oxidation process (SR-AOP) for refractory organic pollutants removal in water. *Chem Eng J*. 2019;378:122149. doi:10.1016/j.cej.2019.12214
9. Ding Y, Wang X, Fu L, et al. Nonradicals induced degradation of organic pollutants by peroxydisulfate (PDS) and peroxymonosulfate (PMS): recent advances and perspective. *Sci Total Environ*. 2021;765:142794. doi:10.1016/j.scitotenv.2020.142794
10. Hou J, He X, Zhang S, Yu J, Feng M, Li X. Recent advances in cobalt-activated sulfate radical-based advanced oxidation processes for water remediation: a review. *Sci Total Environ*. 2021;770:145311. doi:10.1016/j.scitotenv.2021.145311
11. Kang J, Zhang H, Duan X, Sun H, Tan X, Wang S. Nickel in hierarchically structured nitrogen-doped graphene for robust and promoted degradation of antibiotics. *J Clean Prod*. 2019;218:202-211. doi:10.1016/j.jclepro.2019.01.323
12. Hu J, Wang S, Yu J, Nie W, Sun J, Wang S. Duet Fe_3C and FeNx sites for H_2O_2 generation and activation toward

enhanced electro-Fenton performance in wastewater treatment. *Environ Sci Technol*. 2021;55(2):1260-1269. doi:10.1021/acs.est.0c06825
13. Zhou Z, Liu X, Sun K, et al. Persulfate-based advanced oxidation processes (AOPs) for organic-contaminated soil remediation: a review. *Chem Eng J*. 2019;372:836-851. doi:10.1016/j.cej.2019.04.213
14. Sun B, Li Q, Zheng M, et al. Recent advances in the removal of persistent organic pollutants (POPs) using multifunctional materials: a review. *Environ Pollut*. 2020;265(Pt A):114908. doi:10.1016/j.envpol.2020.114908
15. Scheringer M, Salzmann M, Stroebe M, Wegmann F, Fenner K, Hungerbühler K. Long-range transport and global fractionation of POPs: insights from multimedia modeling studies. *Environ Pollut*. 2004;128(1-2):177-188. doi:10.1016/j.envpol.2003.08.027
16. Andreozzi R, Caprio V, Insola A, Marotta R. Advanced oxidation processes (AOP) for water purification and recovery. *Catal Today*. 1999;53(1):51-59. doi:10.1016/S0920-5861(99)00102-9
17. Van der Ploeg F. Natural resources: curse or blessing? *J Econ Lit*. 2011;49(2):366-420. doi:10.1257/jel.49.2.366
18. Morgan JJ. Manganese in natural waters and Earth's crust: Its availability to organisms. In: *Metal Ions in Biological Systems*. CRC Press; 2000.
19. Australian Mines Atlas. Australian Atlas of mineral resources, mines and processing centres. 2016.
20. Ye P, Wang M, Wei Y, Zou Q, Xu A, Li X. Mechanochemical formation of highly active manganese species from OMS-2 and peroxymonosulfate for degradation of dyes in aqueous solution. *Res Chem Intermed*. 2019;45(3):935-946. doi:10.1007/s11164-018-3653-0
21. Wang Y, Xie Y, Chen C, Duan X, Sun H, Wang S. Synthesis of magnetic carbon supported manganese catalysts for phenol oxidation by activation of peroxymonosulfate. *Catalysts*. 2016;7(1):3. doi:10.3390/catal7010003
22. Tian W, Zhang H, Sun H, Tadé MO, Wang S. Template-free synthesis of N-doped carbon with pillared-layered pores as bifunctional materials for supercapacitor and environmental applications. *Carbon*. 2017;118:98-105. doi:10.1016/j.carbon.2017.03.027
23. Wentzell PD, Crouch S. Comparison of reaction-rate methods of analysis for systems following first-order kinetics. *Anal Chem*. 1986;58(13):2855-2858. doi:10.1021/ac00126a059
24. Wang J, Fu Z, Liu G, Guo N, Lu H, Zhan Y. Mediators-assisted reductive biotransformation of tetrabromobisphenol-A by *Shewanella* sp. XB. *Bioresour Technol*. 2013;142:192-197. doi:10.1016/j.biortech.2013.04.062
25. Bai S, Shen X, Zhong X, et al. One-pot solvothermal preparation of magnetic reduced graphene oxide-ferrite hybrids for organic dye removal. *Carbon*. 2012;50(6):2337-2346. doi:10.1016/j.carbon.2012.01.057
26. Tian W, Zhang H, Qian Z, et al. Bread-making synthesis of hierarchically Co@ C nanoarchitecture in heteroatom doped porous carbons for oxidative degradation of emerging contaminants. *Appl Catal B*. 2018;225:76-83. doi:10.1016/j.apcatb.2017.11.056
27. Descostes M, Mercier F, Thromat N, Beaucaire C, Gautier-Soyer M. Use of XPS in the determination of chemical environment and oxidation state of iron and sulfur samples: constitution of a data basis in binding energies for Fe and S reference compounds and applications to the evidence of surface species of an oxidized pyrite in a carbonate medium. *Appl Surf Sci*. 2000;165(4):288-302. doi:10.1016/S0169-4332(00)00443-8
28. Saputra E, Muhammad S, Sun H, Ang H-M, Tadé MO, Wang S. Manganese oxides at different oxidation states for heterogeneous activation of peroxymonosulfate for phenol degradation in aqueous solutions. *Appl Catal B*. 2013;142-143:729-735. doi:10.1016/j.apcatb.2013.06.004
29. Wu H, Xu X, Shi L, et al. Manganese oxide integrated catalytic ceramic membrane for degradation of organic pollutants using sulfate radicals. *Water Res*. 2019;167:115110. doi:10.1016/j.watres.2019.115110
30. Yang Y, Zhang P, Hu K, et al. Sustainable redox processes induced by peroxymonosulfate and metal doping on amorphous manganese dioxide for nonradical degradation of water contaminants. *Appl Catal B*. 2021;286:119903. doi:10.1016/j.apcatb.2021.119903
31. Ye Q. Commodity booms and their impacts on the Western Australian economy: the iron ore case. *Resour Policy*. 2008;33(2):83-101. doi:10.1016/j.resourpol.2007.10.003
32. Hu P, Long M. Cobalt-catalyzed sulfate radical-based advanced oxidation: a review on heterogeneous catalysts and applications. *Appl Catal B*. 2016;181:103-117. doi:10.1016/j.apcatb.2015.07.024
33. Do S-H, Jo J-H, Lee H-K, Kong S-H. Application of a peroxymonosulfate/cobalt (PMS/Co (II)) system to treat diesel-contaminated soil. *Chemosphere*. 2009;77(8):1127-1131. doi:10.1016/j.chemosphere.2009.08.061
34. Shukla P, Sun H, Wang S, Ang HM, Tadé MO. Nanosized Co_3O_4/SiO_2 for heterogeneous oxidation of phenolic contaminants in waste water. *Sep Purif Technol*. 2011;77(2):230-236. doi:10.1016/j.seppur.2010.12.011
35. Awadh SM, Yaseen ZM. Investigation of silica polymorphs stratified in siliceous geode using FTIR and XRD methods. *Mater Chem Phys*. 2019;228:45-50. doi:10.1016/j.matchemphys.2019.02.048
36. Bowden W, Grey C, Hackney S, et al. Lithiation of ramsdellite–pyrolusite MnO_2; NMR, XRD, TEM and electrochemical investigation of the discharge mechanism. *J Power Sources*. 2006;153(2):265-273. doi:10.1016/j.jpowsour.2005.05.059
37. Sugimoto T, Muramatsu A, Sakata K, Shindo D. Characterization of hematite particles of different shapes. *J Colloid Interface Sci*. 1993;158(2):420-428. doi:10.1006/jcis.1993.1274
38. Purushothaman K, Saravanakumar B, Sethuraman B. Inorganic one-dimensional nanomaterials for supercapacitor electrode applications. In: *Morphology Design Paradigms for Supercapacitors*. CRC Press; 2019. doi:10.1201/9780429263347-9
39. Xie G, Liu X, Li Q, et al. The evolution of α-MnO_2 from hollow cubes to hollow spheres and their electrochemical performance for supercapacitors. *J Mater Sci*. 2017;52(18):10915-10926. doi:10.1007/s10853-017-1116-4
40. Hussain S, Amade R, Jover E, Bertran E. Water plasma functionalized CNTs/MnO_2 composites for supercapacitors. *Sci World J*. 2013;2013: 832581. doi:10.1155/2013/832581
41. Han T, Wei Y, Jin X, et al. Hydrothermal self-assembly of α-Fe_2O_3 nanorings@ graphene aerogel composites for

enhanced Li storage performance. *J Mater Sci*. 2019;54(9):7119-7130. doi:10.1007/s10853-019-03371-5

42. Wang H, Mao J, Zhang Z, et al. Photocatalytic degradation of deoxynivalenol over dendritic-like α-Fe_2O_3 under visible light irradiation. *Toxicology*. 2019;11(2):105. doi:10.3390/toxins11020105
43. Liu Y-T, Yuan Q-B, Duan D-H, et al. Electrochemical activity and stability of core–shell Fe_2O_3/Pt nanoparticles for methanol oxidation. *J Power Sources*. 2013;243:622-629. doi:10.1016/j.jpowsour.2013.06.029
44. Meng Y, Wang G, Xiao M, et al. Ionic liquid-derived Co_3O_4/-carbon nano-onions composite and its enhanced performance as anode for lithium-ion batteries. *J Mater Sci*. 2017;52(22):13192-13202. doi:10.1007/s10853-017-1414-x
45. Cheng M, Duan S, Fan H, Su X, Cui Y, Wang R. Core@ shell CoO@ Co3O4 nanocrystals assembling mesoporous microspheres for high performance asymmetric supercapacitors. *Chem Eng J*. 2017;327:100-108. doi:10.1016/j.cej.2017.06.042
46. Qiu B, Guo W, Liang Z, et al. Fabrication of Co_3O_4 nanoparticles in thin porous carbon shells from metal–organic frameworks for enhanced electrochemical performance. *RSC Adv*. 2017;7(22):13340-13346. doi:10.1039/C6RA28296B
47. McAvoy DC, Pittinger CA, Willis AM. Biotransformation of tetrabromobisphenol A (TBBPA) in anaerobic digester sludge, soils, and freshwater sediments. *Ecotoxicol Environ Saf*. 2016;131:143-150. doi:10.1016/j.ecoenv.2015.07.009
48. Lu H, Sui M, Yuan B, Wang J, Lv Y. Efficient degradation of nitrobenzene by Cu-Co-Fe-LDH catalyzed peroxymonosulfate to produce hydroxyl radicals. *Chem Eng J*. 2019;357:140-149. doi:10.1016/j.cej.2018.09.111
49. Wu Y, Li Y, Zhao T, et al. Bimetal-organic framework-derived nanotube@ cellulose aerogels for peroxymonosulfate (PMS) activation. *Carbohydr Polym*. 2022;296:119969. doi:10.1016/j.carbpol.2022.119969
50. Yang Q, Yang X, Yan Y, et al. Heterogeneous activation of peroxymonosulfate by different ferromanganese oxides for tetracycline degradation: structure dependence and catalytic mechanism. *Chem Eng J*. 2018;348:263-270. doi:10.1016/j.cej.2018.04.206
51. Han N, Wang S, Yao Z, et al. Superior three-dimensional perovskite catalyst for catalytic oxidation. *EcoMat*. 2020;3:e12044. doi:10.1002/eom2.12044
52. Ren W, Gao J, Lei C, et al. Recyclable metal-organic framework/cellulose aerogels for activating peroxymonosulfate to degrade organic pollutants. *Chem Eng J*. 2018;349:766-774. doi:10.1016/j.cej.2018.05.143
53. Han N, Yao Z, Ye H, et al. Efficient removal of organic pollutants by ceramic hollow fiber supported composite catalyst. *Sustainable MaterTechnol*. 2019;17:e00108. doi:10.1016/j.susmat.2019.e00108
54. Yan S, Zhang X, Shi Y, Zhang H. Natural Fe-bearing manganese ore facilitating bioelectro-activation of peroxymonosulfate for bisphenol A oxidation. *Chem Eng J*. 2018;354:1120-1131. doi:10.1016/j.cej.2018.08.066
55. Liang H, Sun H, Patel A, Shukla P, Zhu Z, Wang S. Excellent performance of mesoporous Co_3O_4/MnO_2 nanoparticles in heterogeneous activation of peroxymonosulfate for phenol degradation in aqueous solutions. *Appl Catal B*. 2012;127:330-335. doi:10.1016/j.apcatb.2012.09.001
56. Saputra E, Muhammad S, Sun H, Ang H-M, Tadé MO, Wang S. A comparative study of spinel structured Mn_3O_4, Co_3O_4 and Fe_3O_4 nanoparticles in catalytic oxidation of phenolic contaminants in aqueous solutions. *J Colloid Interface Sci*. 2013;407:467-473. doi:10.1016/j.jcis.2013.06.061
57. Kallis G, Butler D. The EU water framework directive: measures and implications. *Water Policy*. 2001;3(2):125-142. doi:10.1016/S1366-7017(01)00007-1
58. WHO. Guidelines for drinking-water quality. WHO Chron. 2011. https://www.who.int/publications/i/item/9789241549950. Accessed 3 October 2022.

How to cite this article: Yao Z, Chen R, Han N, et al. Natural manganese ores for efficient removal of organic pollutants via catalytic peroxymonosulfate-based advanced oxidation processes. *Asia-Pac J Chem Eng*. 2023;18(4):e2907. doi:10.1002/apj.2907